MULTIPHASE FLOW CHARACTERISTICS OF GAS SPARGED HYDROCYCLONE FLOTATION DEINKING

J. D. Miller, A. Das and D. Lelinski
Dept. of Metallurgical Engineering
412 Wm. Browning Building
University of Utah
Salt Lake City, UT 84112

J. W. Chamblee
R & D Engineer
Kamyr Inc.
1 Ridge Center
Glens Falls, NY 12801

ABSTRACT

A new high-efficiency technology has been developed for flotation deinking of various wastepaper grades. The GSC™ gas sparged hydrocyclone is a centrifugal device that operates at consistencies of 1 to 3 percent and uses conventional flotation chemistry.

Research and development efforts have continued in order to better understand the fluid mechanics involved in successful air-sparged hydrocyclone flotation deinking. X-ray computed tomography measurements have helped to describe the multiphase fluid flow in the hydrocyclone, particularly with respect to particle segregation in the swirl flow. This measurement technique has also been used to evaluate the characteristics of the froth phase.

Additionally, bubble size distributions generated during operation of the hydrocyclone have been measured using a special photographic technique. The results of these research efforts will be presented and discussed.

INTRODUCTION

The air-sparged hydrocyclone (ASH) is distinguished by its high specific capacity for fine particle flotation in a centrifugal field. For example, it is now evident that the ASH has a specific capacity of at least 100 times that of conventional flotation equipment. During the 1980s, small, 2-inch diameter ASH units were tested for a large number of mineral commodities, and design modifications were made as necessary (1). The air-sparged hydrocyclone has shown promising potential for the flotation of copper porphyry ore, low-grade placer gold and auriferous pyrite ores, various industrial minerals, and fine coal cleaning. Development efforts have been extended to other countries, including Australia, Brazil, Canada, Chile, Israel, Japan, Mexico, Netherlands, Poland, and South Africa.

One of the promising applications has been found to be the use of the ASH for fine coal flotation. As a result of this pioneering research, the effectiveness of the ASH for fine coal flotation has been demonstrated for a number of U.S. and Canadian coals, and plant-site evaluation of large-diameter units is in progress. Testing of the first 15-inch air-sparged hydrocyclone (ASH-15C) began in October 1992 at the Homer City Coal Preparation Plant and preliminary results indicate that effective separations will be possible for fine coal cleaning.

Also during the last few years, attention has been given to applications of air-sparged hydrocyclone flotation technology outside the mineral industry, including the pulp and paper industry and the food industry, as well as its possible utilization to solve environmental problems (oil spills, soil remediation, hazardous waste, etc.). The most significant development, however, was the construction in 1991 of a wastepaper recycling pulp mill which uses air-sparged hydrocyclone technology for deinking flotation. The plant, which began operation in June 1992, employs a 3 stage flotation system using twenty 6-inch ASH units to produce 120 ADT/day of recycled market pulp (2, 3).

In addition to these efforts to commercialize the ASH technology, fundamental research has been on-going, and currently x-ray computed tomography studies of the time-averaged multiphase flow characteristics are being supported by NSF and DOE. As a result of these x-ray CT studies, a better appreciation of the influence of system variables on the nature of the segregated flow is being developed. In addition, high-speed photography and high-speed video techniques are being used to examine the nature of bubble formation in the swirl flow of the ASH and the corresponding bubble size distributions. On this basis, it is expected that these fundamental measurements will help to establish design features and operating conditions for even more efficient flotation separations.

PRINCIPLES AND DESIGN FEATURES

The basic concept from which high-capacity air-sparged hydrocyclone flotation evolved was the notion that fine hydrophobic particles are difficult to float because they have insufficient inertia to penetrate/rupture the bubble film and establish a stable attachment with the bubble. In this regard, if the fine particles' inertia could be increased by placing it in a centrifugal force field, more effective flotation of fine particles could be realized. Such a centrifugal force field is found for the fluid flow in hydrocyclone separators. A number of designs for the air-sparged hydrocyclone were tested in the early eighties, and as a result a preferred design, a vertically oriented, cylindrical cyclone with a tangential feed entry at the top, was established (4). A schematic drawing of such an air-sparged hydrocyclone is

presented in Figure 1. The ASH unit consists of two concentric right-vertical tubes, a conventional cyclone header at the top, and a froth pedestal at the bottom. The inner tube is a porous wall through which air is injected. The outer nonporous tube simply serves as an air jacket to provide for even distribution of air through the porous inner tube. The slurry is fed tangentially through the conventional cyclone header to develop a swirl flow of a certain thickness in the radial direction (called the swirl layer thickness) adjacent to the porous wall, leaving an air core centered on the axis of the air-sparged hydrocyclone. The swirl flow thus created shears the injected air to produce a high concentration of small bubbles. In wastepaper flotation, hydrophobic ink particles in a pulp suspension collide with these air bubbles, and after attachment, lose some of their tangential velocity, and are transported radially into a froth phase which forms at the surface of the air core on the cyclone axis. The froth phase is stabilized and constrained by the froth pedestal at the underflow and thus moves towards the vortex finder of the cyclone header and is discharged as an overflow reject stream. Hydrophilic particles including pulp fibers generally remain centrifuged at the porous tube wall and are accepted through the annular underflow opening created between the inner porous tube wall and the froth pedestal (5).

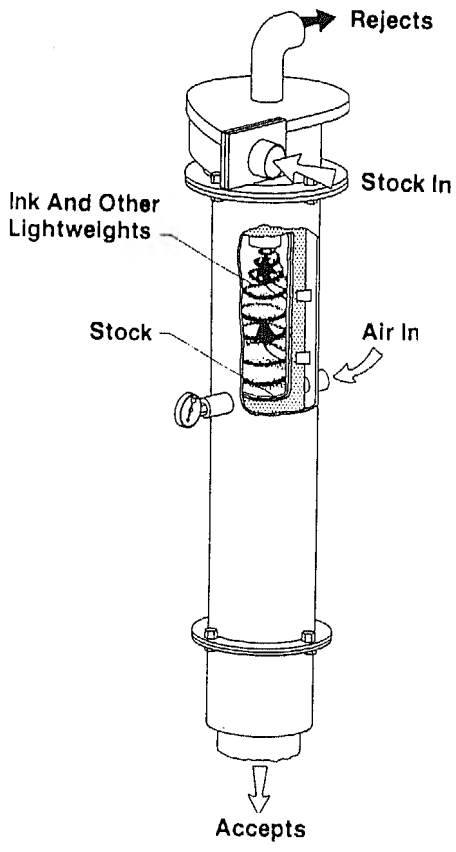

Figure 1. Perspective of the air-sparged hydrocyclone (ASH).

The design features of the ASH improve the floatability of fine ink particles in two ways. First, a significant centrifugal force field is developed, the magnitude of which is determined by the slurry feed rate and the cyclone diameter. This centrifugal force field results in increased inertia of fine ink particles and hence facilitates their attachment to air bubbles. Secondly, the high-speed swirl flow creates a significant shear force at the porous wall, which shears the air injected through the porous tube into numerous small air bubbles, thus increasing the rate of flotation of fine hydrophobic ink particles. Further, these small air bubbles are directed in the radial direction, orthogonal to the motion of the hydrophobic ink particles in the swirl flow. As a result, the probability of collision of air bubbles with hydrophobic ink particles is significantly increased, and effective flotation of these fine ink particles can be achieved for residence times that approach the intrinsic bubble/particle attachment times. Consequently, a specific flotation capacity on the order of 30 tpd/ft^3 of cyclone volume is realized, at least 100 times the specific capacity of conventional mechanical or column flotation cells.

MULTIPHASE FLOW CHARACTERISTICS BY X-RAY COMPUTED TOMOGRAPHY

During the past few years research efforts have been made to examine time-averaged multiphase flow in air-sparged hydrocyclone flotation by x-ray computed tomography. In x-ray CT an x-ray beam of intensity I_0 is incident on an object and emerges with an intensity I. The measurement quantity (I/I_0) is equal to the summation of the x-ray attenuation coefficients of the material at each point along the incident line. Total attenuations are measured along all rays through an object from several directions around the object, and the image is reconstructed from these intensity data using a reconstruction algorithm. The computer software, according to this specific algorithm, manipulates the measured projections and produces a two-dimensional map of x-ray attenuation coefficients (CT numbers) of the irradiated cross sections. The attenuation coefficients are correlated with density by calibrating the CT machine with objects of known density and obtaining a correlation equation that relates attenuation coefficients and thus CT numbers with density. In such a fashion, then quantitative x-ray CT measurements are possible and a two-dimensional density map of the object under investigation is established (6, 7).

Already, preliminary results using a quartz (120 microns)

suspension as a model system have clarified certain aspects of the flow and provided valuable information on the geometric characteristics of the air core, the froth phase and the swirl layer. The narrow size quartz system was selected to facilitate the contrast between the froth phase and swirl layer and thus allow for x-ray CT analysis. Generally, these preliminary results substantiate previous inferences regarding the nature of multiphase flow during ASH flotation.

A reconstructed CT image and the corresponding time-averaged radial density profile is presented in Figure 2. Darker regions in the image identify the regions of higher density. During ASH flotation, three regions, namely, the air core, the froth phase and the swirl layer, can be identified as indicated in the radial density profile shown in Figure 3. A transition region between the froth phase and the swirl layer as had been suggested previously is not well defined, but the possibility of its existence should not be neglected.

Flow Geometry

The geometric features of the multiphase flow can be summarized in more detail by referring to Figures 3-5, which for each figure shows three cross sectional scans at the top, middle and bottom of the ASH (experimental details are provided in the caption). Actually, 11 scans were taken for each experiment.

Of course, the tangential velocity decreases from top to bottom because of the swirl decay. Thus, the centrifugal force is maximum at the top and minimum at the bottom. This feature is generally reflected in the air core dimension. Examination of the images presented in Figure 3, shows that the air core radius is greater at the top of the ASH than that at the bottom. At the top the air core radius is 9.1 mm and decreases to 7.2 mm at the bottom. Investigation of all CT image data reveals that in most cases the shape of the air core is conical. Observations regarding air core radius have been summarized in Table 1. For 5% solids in the feed (feed density 1.032 g/cc), the air core radius at the top was observed to decrease with an increase in A*, the dimensionless ratio of the overflow opening area (vortex finder diameter) to the underflow opening area (annular opening created by froth pedestal). In this way the magnitude of A* is changed mechanically and does not depend on flow conditions. It is clear from Table 1 that the air core volume is a maximum for the smallest A* value considered (A* = 0.74).

High percent solids in the feed slurry is characterized by a smaller air core and the conical shape is no longer well defined. Instead, the air core takes on a cylindrical shape as is evident from the data presented in Table 1. With 15% solids (feed density = 1.104 g/cc), the air core radius varied from 2.2 to 7.0 mm depending on experimental conditions. Without any collector addition, the air core radius at the top decreased from 5.1 mm to 2.2 mm as A* increased from 0.74 to 1.00; again indicating that the air core volume is greatest for the smallest A* value under consideration. When collector was added, the air core radius remained approximately the same for all three A* values which suggests that the air hold up is comparable in these three cases. This is easily seen from the images presented in Figure 5.

Air Flow Distribution

In view of the results discussed in the previous section, it appears from the analysis of the air core dimensions that the axial air flow distribution is not uniform during flotation. This analysis is supported by the variation in density and thickness of the swirl layer as can be seen in Figures 3, 4 and 5. It is evident from these figures that the thickness of the swirl layer is smaller at the top than that at the bottom.

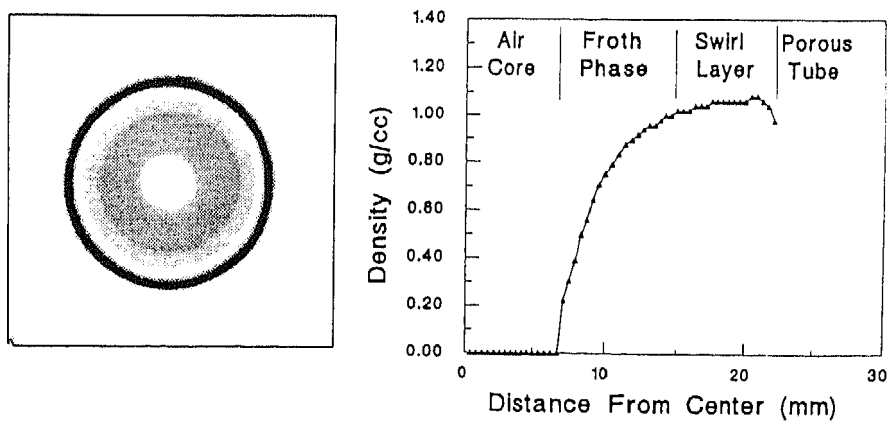

Figure 2. A reconstructed CT image at the top of the ASH and the corresponding radial density profile.

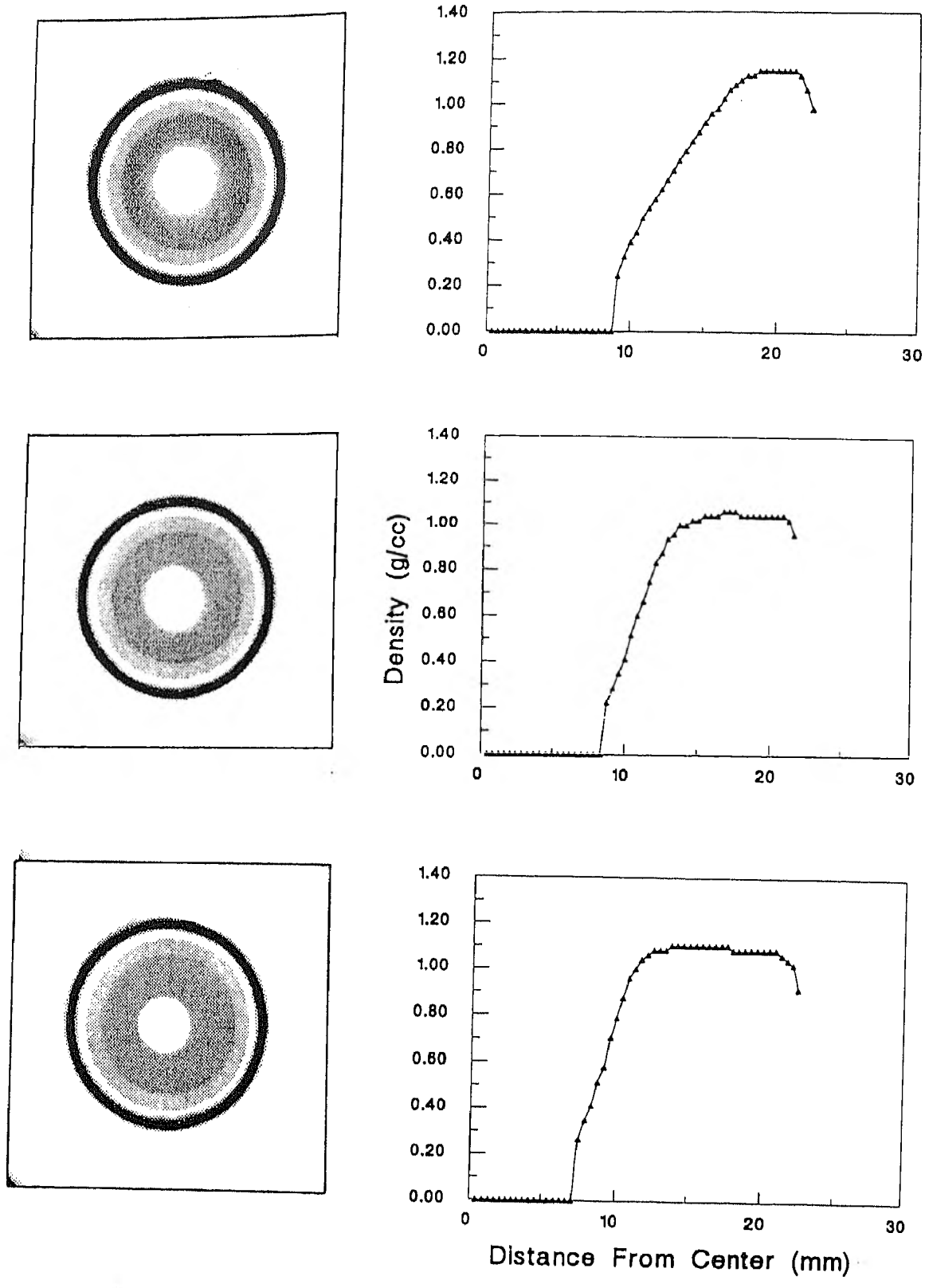

Figure 3. CT images and radial density profiles for quartz (100×200 mesh) suspension at the top, middle and bottom of the ASH-2C for 5% solids (feed density = 1.032), 800 g/t collector and A* = 1.00.

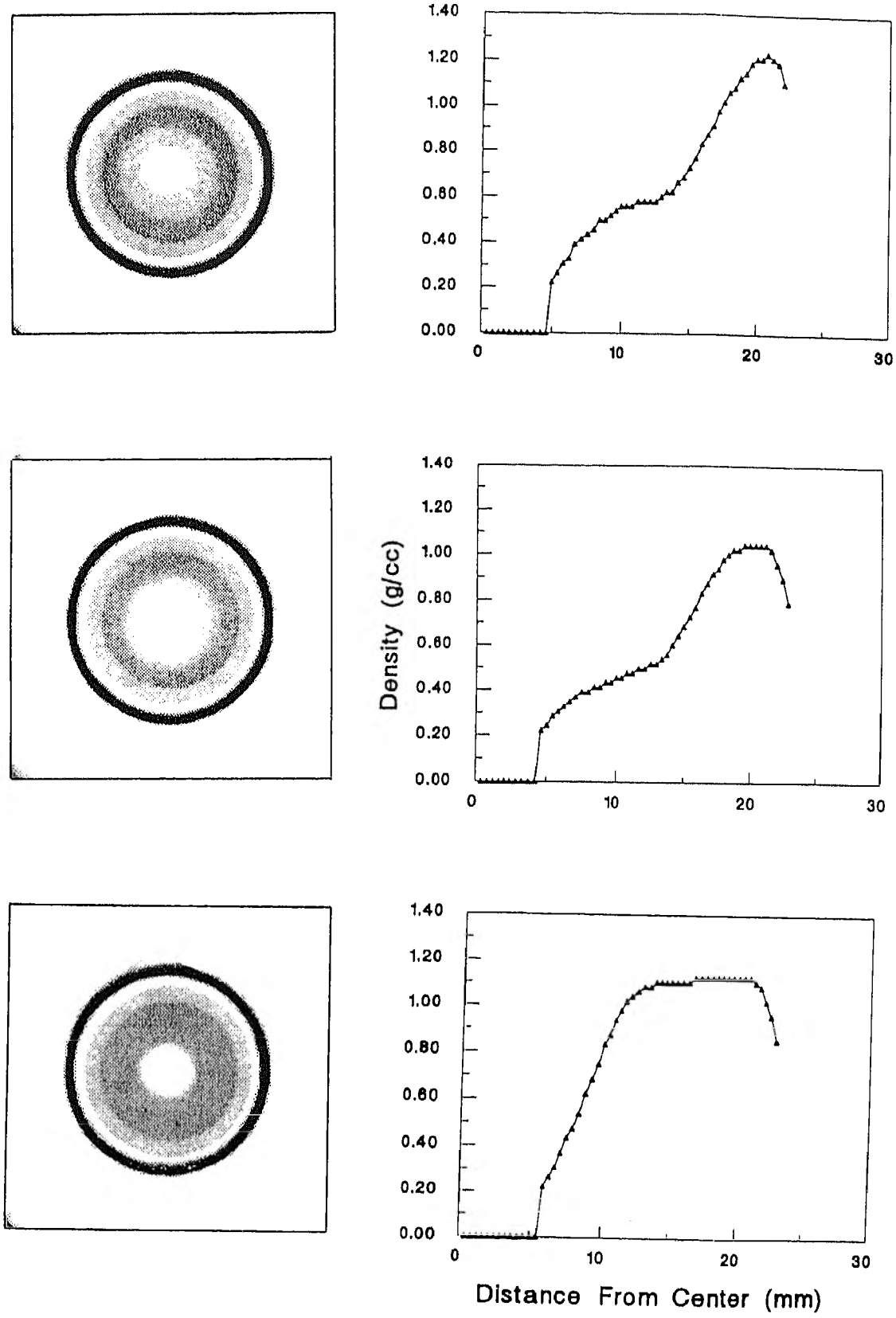

Figure 4. CT images and corresponding radial density profiles for quartz (100×200 mesh) suspension at the top, middle and bottom of the ASH–2C for 15% solids (feed density = 1.104), no collector and A* = 0.85.

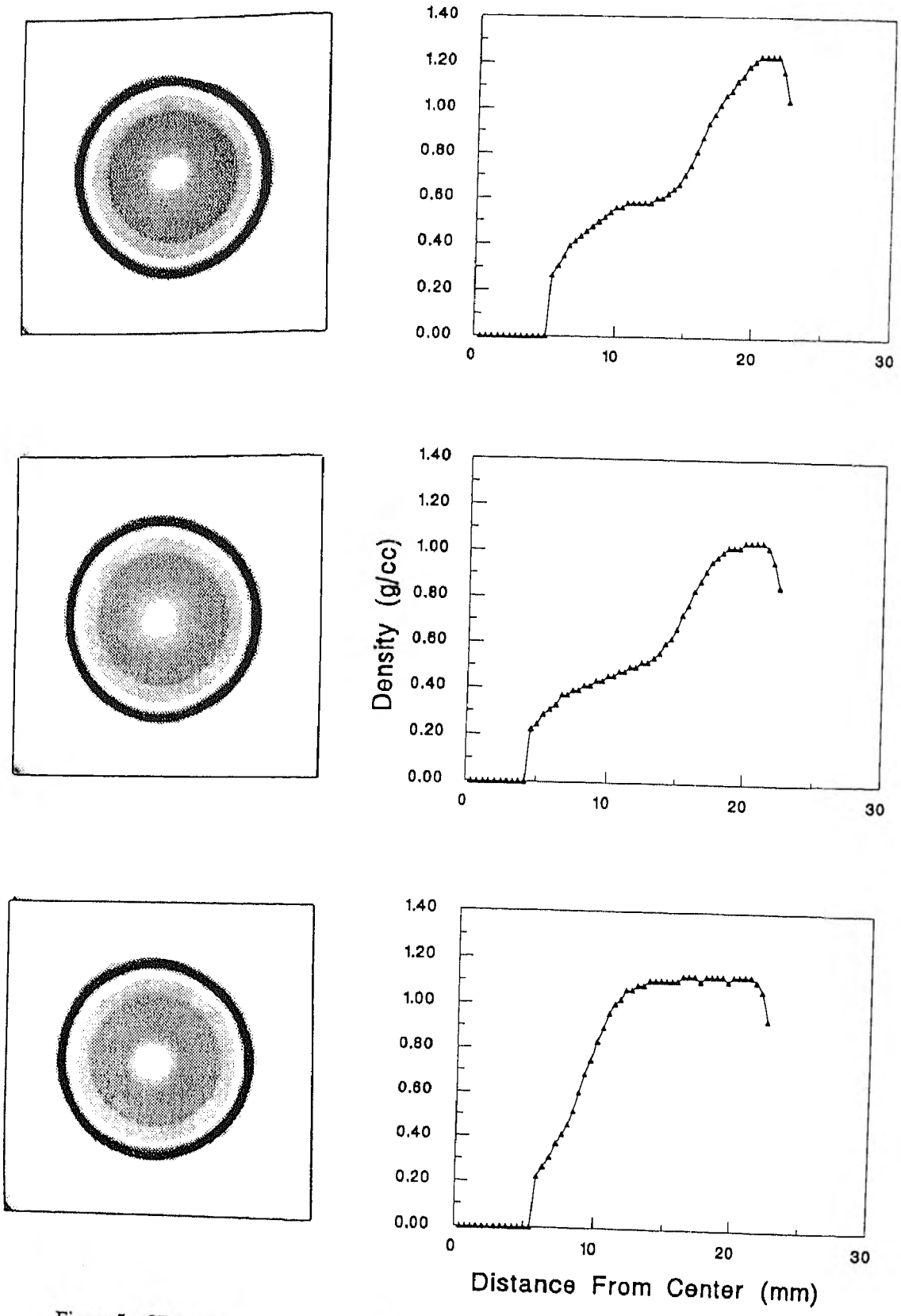

Figure 5. CT images and corresponding radial density profiles for quartz (100×200 mesh) suspension at the top, middle and bottom of the ASH-2C for 15% solids (feed density = 1.104), 800 g/t collector and A* = 1.00.

Table 1. Radius of the air core at different locations for quartz (120 microns) suspension under various experimental conditions.

Solids (%)	A*	Collector (g/ton)	Air Core Radius Top (mm)	Middle (mm)	Bottom (mm)
5	0.74	0	12.0	11.0	8.0
5	0.85	0	8.7	8.0	7.0
5	1.00	0	6.2	7.5	6.0
5	0.74	800	13.3	9.1	8.5
5	0.85	800	9.5	8.7	8.0
5	1.00	800	9.1	8.6	7.2
15	0.74	0	5.1	4.0	5.1
15	0.85	0	4.9	4.1	5.2
15	1.00	0	2.2	2.6	2.5
15	0.74	800	5.0	4.1	5.1
15	0.85	800	7.0	6.4	4.9
15	1.00	800	5.0	4.3	5.1

Further the density of the swirl layer is greatest at the top of the ASH. The swirl layer, because of the higher centrifugal force, is in a compact state at the top, resulting in a higher density (lower hold up of air) whereas the swirl layer is expanded at the bottom and is of a lower density due to greater hold up of air. It is believed that these results are indicative of a greater air flow through the bottom of the ASH. Such an interpretation can be rationalized by the fact that the resistance to air flow at the bottom will be less due to the reduction in the tangential velocity component of the swirl flow and thus a reduced centrifugal force. In this regard, multiple air chambers have been used to shift the air flow distribution patterns when necessary.

Particle Hydrophobicity

Since the quartz particles (-100 +200 mesh) are naturally hydrophilic, the solid split to the overflow (OF) rejects is negligible (about 0.5% of the feed solids; at 5% solids in the feed and a feed density of 1.032). In the absence of collector addition, essentially all of the quartz is found in the underflow (UF) accepts. For 5% solids in the feed slurry and no collector, the water split to the OF rejects was observed to increase with an increase in A*. Experimental data regarding solids and water split to the OF rejects for various experimental conditions are summarized in Table 2. Notice that with the addition of 800 g collector (amine) per ton of quartz, the quartz particles become hydrophobic. Excellent ASH flotation takes place as is evident from Table 2. For 5% solids in the feed the solids split to OF rejects was found to increase from 68.4% to 85.6% and finally to 94.2% with an increase in A* from 0.74 to 0.85 and finally to 1.00 respectively. The radial density profiles with collector addition are presented in Figure 3 for 5% solids. A higher density for the froth phase indicates that hydrophobic quartz particles were transported into the froth phase. Near the top, the density of the froth phase increases gradually from the air core to the swirl layer which is estimated to be about 6 mm in thickness, whereas at the bottom, the froth phase is narrow (about 5 mm) and the density rises abruptly indicating that the froth phase near the bottom is depleted of the hydrophobic quartz particles. These results clearly show that froth transport to the vortex finder is excellent at A* = 1.00. However, for smaller A* values (0.74 and 0.85) some hydrophobic quartz particles are found in the UF accept stream.

When no collector was added, the solids split to the OF reject stream with 15% solids in the feed slurry was in the range of 1–3% for different values of A*. The water split to the OF rejects was 20.63, 26.95 and 36.22% for A* values of 0.74, 0.85 and 1.00 respectively as can be seen from Table 2. The addition of collector (800 g amine per ton of quartz) resulted in substantial flotation and transport of hydrophobic quartz particles to the overflow rejects. The solids split to the OF rejects was found to be 15.5%, 50.9% and 97.3% for A* values of 0.74, 0.85 and 1.00 respectively. It is evident that higher A* values improve quartz flotation.

Table 2. Water split and solids split to the overflow rejects for quartz (120 microns) suspension under various experimental conditions.

Solids (%)	A*	Collector (g/ton)	Water split to OF Rejects (%)	Solids split to OF Rejects (%)
5	0.74	0	9.40	0.31
5	0.85	0	17.54	0.49
5	1.00	0	23.72	0.62
5	0.74	800	7.58	68.42
5	0.85	800	12.23	85.55
5	1.00	800	18.48	94.23
15	0.74	0	20.63	3.07
15	0.85	0	26.95	2.91
15	1.00	0	36.22	1.38
15	0.74	800	11.61	15.51
15	0.85	800	15.81	50.91
15	1.00	800	15.52	97.25

The density profiles and CT images for this case are presented in Figure 3. For A* = 1.00, the plateau region, indicative of the swirl layer thickness, is very wide near the bottom and has an average density of about 1.0 g/cc. On the other hand, at the top, the plateau is narrow and the gradual rise in density from the froth phase to the swirl layer is notable. These results indicate the presence of hydrophobic quartz particles in the froth phase at the top of the ASH, and excellent flotation is realized (8). However, for lower A* values the plateau region is smaller even at the bottom and the rise in density through the froth phase is not abrupt. These results show that some solids are still being accepted to the UF for lower A* values (A* = 0.74, 0.85). Testing with pulp slurries has yielded similar results except that the high water split observed at low collector dosage is accompanied by high fiber losses to the OF reject stream.

BUBBLE SIZE DISTRIBUTIONS

In addition to the study of multiphase flow by X-ray CT, R&D efforts have included studies to determine bubble size during air-sparged hydrocyclone flotation. Bubble size is always of interest in the analysis of flotation separations, and many researchers believe that bubble size is a critical factor which controls the rate of flotation and the efficiency of separation. Bubble size measurement during ASH flotation is rather difficult. Several theoretical approaches have been used to estimate the average bubble size. Also experimental high-speed video measurements of bubble size for bubble production from a single capillary have been reported for a model swirl flow system (1). It was found that the bubble size was comparable to the capillary diameter and did not change with the air flowrate. These results were in general agreement with theory. It was found in this model swirl flow system that the surface tension (frother concentration) did not influence the bubble size generated from a single capillary because of jet formation.

In order to improve our understanding of bubble formation during ASH flotation, measurements were carried out to determine the bubble size distributions in the underflow stream during water-only operation of actual ASH units of different diameter and different length. The effect of pore size has not yet been studied in detail. A high-speed photographic technique was used, and the system included a Pentax K1000 35–mm camera with a Samyang 28–200 mm lens. A Vivitar 283 electronic flash coupled with a reflecting screen allowed for a 30–μs exposure time. The froth pedestal of the ASH was replaced by a 90° plexiglas cone to improve resolution of the bubbles. Nevertheless, due to the velocity of discharge ($\sim$1 m/sec) and the limitations of the photographic system, the detection of bubbles smaller than 300 μm was difficult. The photographs of the underflow stream were taken just as the water discharged from the ASH. The significance of bubble coalescence was evaluated from variations in the length of the ASH. The effect of frother, 4–methyl–2–pentanol (MIBC), was studied at concentrations from 0 to 20 mg/L.

Frother Concentration

Typical air bubble size distributions for different frother concentrations are presented in Figure 6. When the frother concentration increases the size distribution becomes narrower and shifts towards smaller average bubble diameters. These results confirm earlier predictions for bubble generation from a porous wall under significant shear (9). In the absence of frother the distribution shows a characteristic contribution from both large and small bubbles. It is believed that the large bubbles were formed by coalescence, and that the fine bubbles are, in part, the satellite bubbles released during the formation and/or coalescence process.

The concentration of frother had the most pronounced effect on the average bubble size as calculated from each size distribution. See Figure 7. The average bubble size dropped from almost 1000 μm to below 500 μm with an increase in frother concentration for 0 ppm to 20 ppm. Such a change in the bubble size was not observed during the swirl flow study of bubble formation from a single capillary. It may be that the major role of the frother is to prevent coalescence of bubbles as they form at adjacent pores on the porous tube wall. Also it was observed that with an increase in frother concentration the bubble concentration in the underflow accepts increased, presumably due to smaller bubble diameters and greater retention in the swirl layer.

ASH Diameter

The average diameter of bubbles generated in the 15-cm ASH-6C unit was approximately 25% larger than in the 5-cm ASH-2C unit when frother was absent, as is evident from the data presented in Figure 7. With an increase in MIBC concentration the bubble size decreased in both ASH units, and the difference in the average bubble size diminished. For example, for the 5-cm unit (47 cm in length, Q^* = 2) the average bubble size dropped from 780 μm at 0 ppm MIBC to 420 μm at 20 ppm MIBC, whereas for the 15-cm unit (117 cm in length, Q^* = 2) the average bubble size dropped from 890 μm at 0 ppm MIBC to 440 μm at 20 ppm MIBC. At higher frother concentration the bubble size is almost independent of ASH diameter, and from one perspective this might be attributed to the fact that as the bubbles become smaller the thickness of the effective hydrodynamic boundary layer for the swirl flow is no longer of significance. In the absence of frother the bubble size is sufficiently large that the bubble extends beyond the effective boundary layer into the shear flow. In this way, the shear velocity which, of course, is greater for the 5-cm ASH-2C unit leads to smaller bubbles for the 5-cm ASH-2C unit in the absence of frother. On the other hand in the presence of sufficient frother bubble release occurs at a smaller size in the boundary layer due to a reduced surface tension, and the boundary layer thickness (ASH diameter), under these circumstances, does not significantly influence bubble size. In addition the presence of frother tends to stabilize these smaller bubbles and prevent coalescence. Of course, the effect of frother is of considerable significance and quite different from the results reported for single capillary experiments.

ASH Length (L)

The data presented in Figure 7 indicate that the length of the ASH unit has no influence on the measured bubble size for both 5-cm and 15-cm ASH units. These results suggest that coalescence after formation is not significant and that the measured bubble size in the underflow is probably close to the bubble size in the swirl layer.

Dimensionless Flowrate Ratio (Q^*)

Of equal importance from these results is the observation that the bubble size distribution is independent of the dimensionless flowrate (Q^* = air flowrate/water flowrate) for both the 5-cm ASH-2C unit and the 15-cm ASH-6C unit for all concentrations of MIBC as shown in Figure 8. Strictly speaking, the water flowrate remained constant (at 70 lpm for the 5-cm ASH-2C unit and at 700 lpm for the 15-cm ASH-6C unit), and only the air flowrate was changed. The lack of influence of air flowrate on bubble size was already predicted for air-sparged hydrocyclone flotation, and regarding bubble generation from orifices, these findings support the findings from previous research for orifice air velocities exceeding 0.1 m/s (10).

Discussion

The experimental results from bubble size measurements can be discussed in terms of frother stabilization of bubbles formed at individual pores and the effective thickness of the hydrodynamic boundary layer relative to bubble size. Such an analysis has been discussed in preceding sections.

On the other hand, it may be imagined that air is injected as numerous small jets of air, perhaps 1 mm in length, emanating from active pores typically 50 μm in diameter. The air jets are broken, and the bubbles thus formed are accelerated through the swirl flow due to their buoyancy and the centrifugal force field. The bubble size might then be expected to be controlled more by the size of the turbulent eddies rather than by the pore size of the porous tube.

Finally, it should be remembered that measurement of bubble sizes of less than 100 μm was not possible with the equipment used, and further research must be undertaken with an improved photographic system.

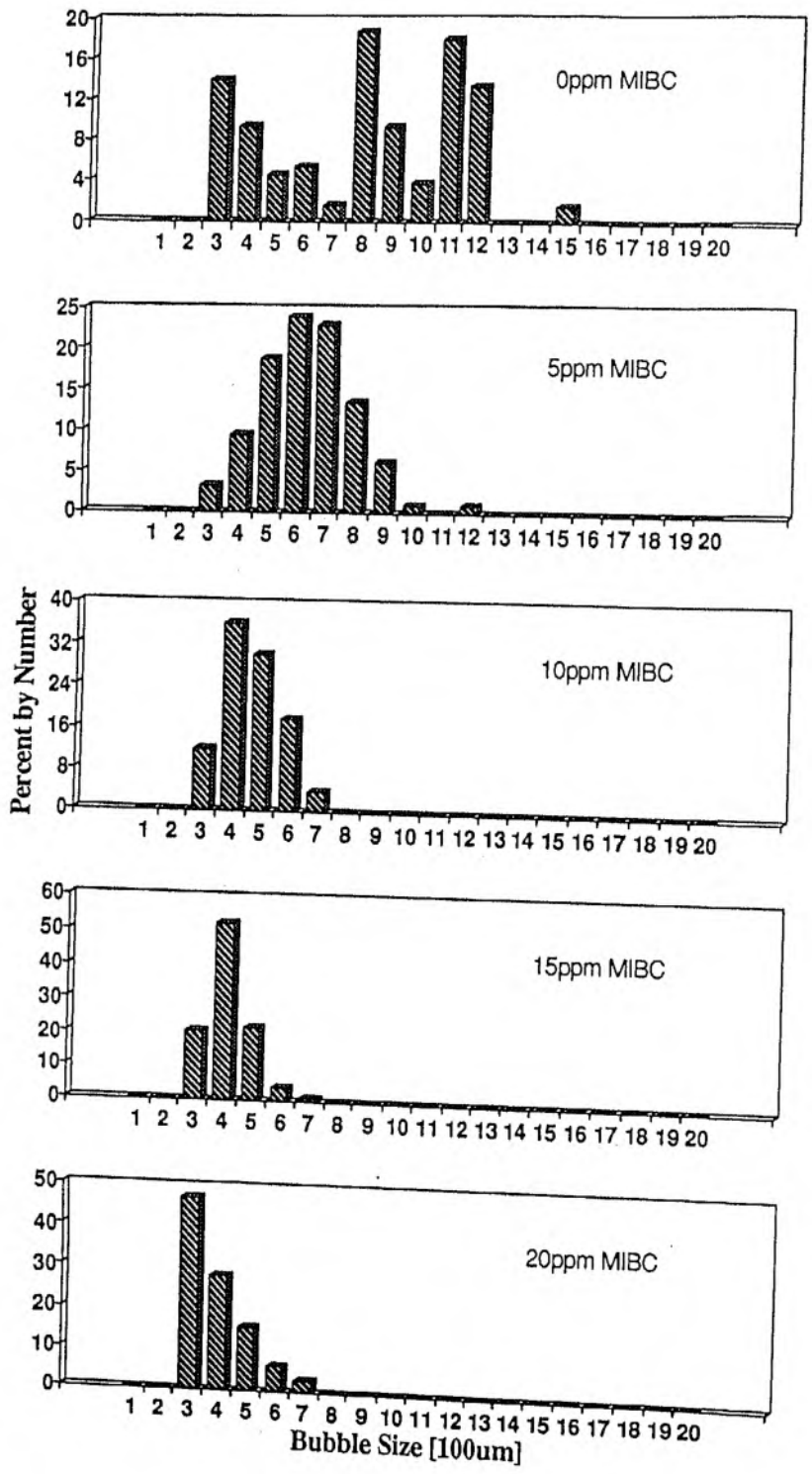

Figure 6. The size distribution for air bubbles leaving the ASH in the underflow as a function of MIBC concentration, measurements were made for 5–cm dia., 16–cm long ASH.

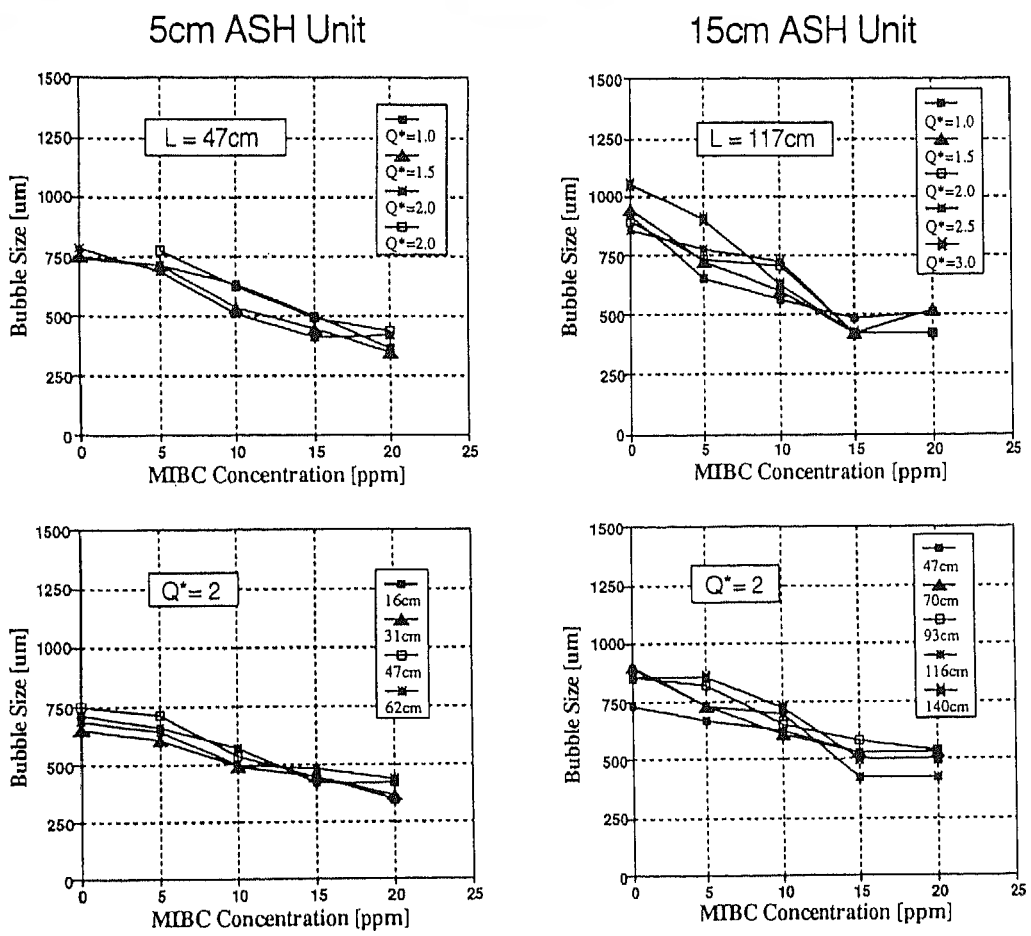

Figure 7. Average bubble size in the underflow as a function of MIBC concentration for 5-cm ASH and 15-cm ASH units of different lengths (L) and different dimensionless flowrate ratios (Q*).

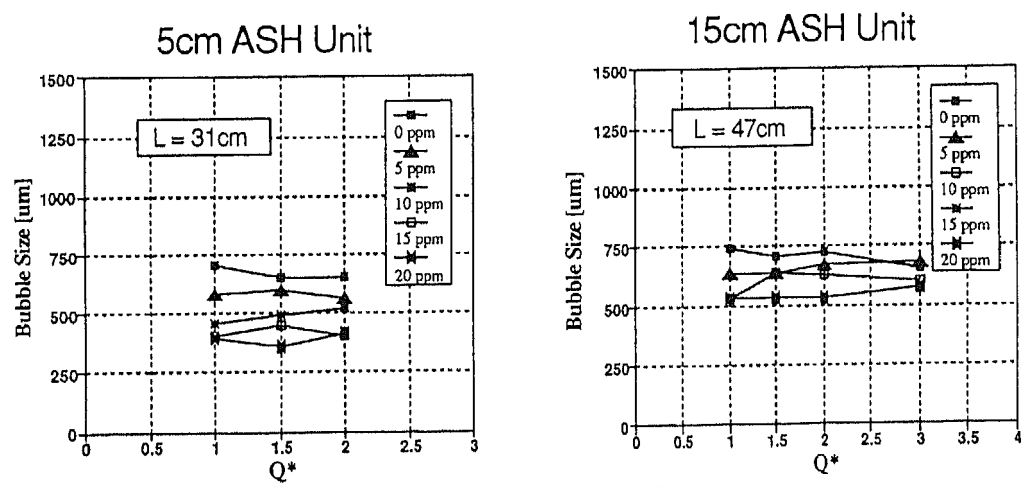

Figure 8. Average bubble size in the underflow as a function of the dimensionless flowrate ratio (Q*) for 5-cm ASH and 15-cm ASH units of different lengths (L) and for different MIBC concentrations.

SUMMARY AND CONCLUSIONS

Progress continues to be made in the development of air-sparged hydrocyclone (ASH) flotation technology. Significant strides have been made in the commercialization of the ASH technology, while R&D efforts have added to our understanding of this complex flotation phenomenon. In addition to defining flow geometry, it appears that x-ray CT measurements will provide very useful density profile information regarding phase distribution, particularly with respect to the recovery of hydrophobic particles. Other R&D activities include efforts to measure bubble size distributions by photography using a high-speed flash.

ACKNOWLEDGEMENTS

Appreciation is given to K. Argyle and K. Cundick for assistance in the preparation of this paper. Support for fundamental study of air-sparged hydrocyclone flotation is being provided by NSF, CTS-9000406, and DOE, DEFG-2290PC90311, and is gratefully acknowledged.

REFERENCES

1. Miller, J. D. and Ye, Y., 1989, "Froth characteristics in air-sparged hydrocyclone flotation," *Mineral Proc. & Extr. Metallurgy Rev.*, pp. 307–329, vol. 5.

2. Chamblee, J. W., and Greenwood, B. F., 1991, "Evaluation of High Throughput High Consistency Deinking Technology," TAPPI Pulping Conference, Nov. 4–7.

3. Chamblee, J. W., and Plattner, G., 1992, "Gas Sparged Cyclone Flotation Processes," TAPPI Pulping Conference, Boston, Nov. 1–6.

4. Miller, J. D. and Kinneberg D. J., 1984, "Fast flotation in an air-sparged hydrocyclone," *Proc. of MINTEK 50*, pp. 373–383, South Africa, vol. 1, March, 1984.

5. Yu, Q., Ye, Y., and Miller, J. D., "Dispersion and aggregation of newspaper pul pfor fiber recovery by deinking with air-sparged hydrocyclone flotation," *Proceedings of the Engineering Foundation Conference on Dispersion and Aggregation: Fundamentals and Applications*, Palm Coast, Florida, March 1992.

6. Miller, J. D., Lin, C. L., and Cortes, A. B., 1990, "Review of X-Ray Computed Tomography and Its Applications in Mineral Processing," *Mineral Processing and Extractive Metallurgy Review*, Vol. 7, pp. 1–18.

7. Miller, J. D., Lin, C. L., and Cortes, A. B., 1991, "An Improved X-Ray CT Reconstruction Algorithm Suitable for Quantitative Analysis in Industry Applications," *Review of Progress in Quantitative NDE*, Proceedings of the 17th Annual Conference, July, 1990, La Jolla, CA; Vol. 10A, ed. by D. O. Thompson and D. E. Chimenti, Plenum, New York, pp. 459–467.

8. Miller, J. D., and Das, A., 1992, "X-Ray CT Analysis of Multiphase Flow during ASH Flotation," to be published.

9. Miller, J. D., Upadrashta, K. R, Kinneberg, D. J., and Gopalakrishnan, S., 1985. "Fluid-flow phenomena in the air-sparged hydrocyclone," *XV Int. Mineral Proc. Cong.*, pp. 87–99, Cannes, July 2–9.

10. Saxena, S. C., Patel, D., Smith, D. N., and Reuther, J. A., 1988, "An assessment of experimental techniques for the measurement of bubble size in a bubble slurry reactor as applied to indirect coal liquefaction," *Chem. Eng. Comm.*, pp. 87–127, vol. 63.